IEEE Access
Multidisciplinary | Rapid Review | Open Access Journal

Received March 23, 2021, accepted April 20, 2021, date of publication April 27, 2021, date of current version May 6, 2021.

*Digital Object Identifier 10.1109/ACCESS.2021.3076006*

# A Method of D-Type Weld Seam Extraction Based on Point Clouds

**JIE GAO, FANG LI, CONG ZHANG, WENHAO HE, JINHU HE, AND XUBING CHEN, (Senior Member, IEEE)**

School of Mechanical and Electrical Engineering, Wuhan Institute of Technology, Wuhan 430205, China

Corresponding authors: Fang Li (lifang@wit.edu.cn) and Xubing Chen (chenxb@wit.edu.cn)

This work was supported in part by the National Natural Science Foundation of China under Grant 51875415, and in part by the Natural Science Foundation of Hubei under Grant 2019CFA026.

**ABSTRACT** Identification of the seam to be welded in automatic welding is an important challenge, especially on a complex 3D surface. At present, most studies on weld extraction are for butt joints and fillet joints. Few studies focus on D-type welds, which connect to pipelines or pressure vessels. In this paper, a method of identification and extraction of pipeline joint welds based on 3D point clouds is proposed. First, the problem that the surface of pipe fittings cannot be effectively stitched owing to lack of markings is solved by putting marker points on the surface to allow accurate splicing of the point cloud. Second, according to the contour feature information of the workpiece, a processing method for D-type welding seams is proposed. Finally, a boundary extraction algorithm based on the point cloud normal is used to obtain the point cloud of the weld. The experimental results show that this method can effectively extract the weld. The running time for the point cloud weld extraction method is less than half that of the existing methods. The accuracy of the proposed method is improved in all three directions: by 28.2% in the X direction, 19.1% in the Y direction and 16.0% in the Z direction. Moreover, this method is convenient for transforming weld coordinates to robot-based coordinates for the automatic welding of spatially complex welds.

**INDEX TERMS** D type weld seam, feature extraction, point cloud, automated welding.

## I. INTRODUCTION

Welding of metals plays a vital role in industrial manufacturing. D-type welds, which are welds where the joint crosses the vessel, can have highly concentrated stress. A full-penetration weld is often used, which can be difficult to produce. Figure 1 shows examples of this type of weld. Such welds are mostly made automatically, and are commonly found in pressure vessels, which impose high requirements on weld quality [1]. The welding process is complicated by many factors, including welding dust, the arc light and the nature of the melt pool. The welding process has time-varying, nonlinear and uncertain characteristics, which make it difficult to establish an accurate mathematical model for automatic weld tracking. Therefore, tracking the weld trajectory automatically using sensors is required. The accurate identification and extraction of the weld trace on a complex-shaped surface is key to this. Kong and Dai [2] proposed a three-point weld location method based on structured light vision. Li [3] applied an image processing method based on morphology and Canny algorithm to identify and extract the weld – however, this method is only suitable for flat welds. Based on binocular vision sensors, Wang and Lv [4] performed stereo matching of weld images to obtain the shape of a spatial weld, to within an error of 10%.

However, the binocular or multiocular stereo vision systems used to collect 3D information have many disadvantages: high cost, large size, complex extraction of feature points from images, and complex matching algorithms. They require calibration between multiple cameras, which can be affected by changes in the external environment. Furthermore, this can make the result unstable [5]. An alternative approach is to adopt point clouds to take the depth information about the parts to be welded (i.e., the distances between the part and sensors), and process these point clouds to directly obtain the coordinate points of the welding seam. [6] The processing algorithms for point cloud data, including point cloud filtering, feature extraction algorithm, and registration, have already been developed. For example, Liu *et al.* [7] adopted the kernel density estimation clustering

The associate editor coordinating the review of this manuscript and approving it for publication was Chi-Tsun Cheng.

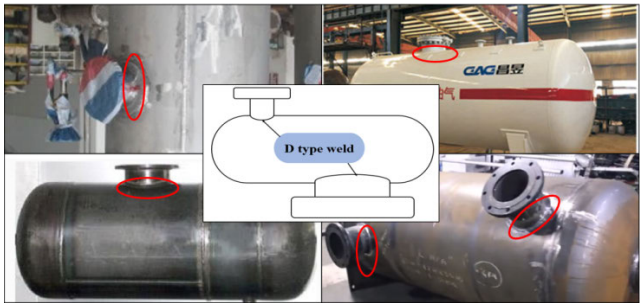


**FIGURE 1.** Space sealing welds to pressure vessels (D-type welds).

method and set the threshold to filter outliers, to achieve smooth denoising of point cloud data, whereas the iterative nearest point algorithm (ICP) [8] is the most widely used point cloud registration algorithm at present. Guo *et al.* [9] used a genetic algorithm to improve the efficiency of solving practical problems with point clouds, and Yan *et al.* [10] also adopted a genetic algorithm for global optimization along with ICP local optimization to improve the accuracy of point cloud matching.

Building on this, point cloud methods are gradually being applied to extract welding information. Njastad [11] used a Kinect camera as a point cloud device to obtain images of parts prior to welding, and then matched the point cloud to a CAD model to obtain a highly accurate location of the welding seam. However, the weld in this experiment was planar. Bredvold *et al.* [12] also used a Kinect to obtain a point cloud of the workpiece, a cylindrical pipe with a weld seam connecting two segments. Stéphane and Margit [13] was used to slice the point cloud of the workpiece to obtain the completed cylindrical weld track. However, the Kinect camera had low resolution, and the point cloud acquisition had errors.

The remainder of this article is arranged as follows: Section 2 introduces the theory of methods to extract D-type weld information. A method for splicing point clouds of workpieces lacking feature information is proposed. Methods to process the weld point cloud and extract the weld are then proposed. The third section describes our experimental verification of the reliability of the algorithm. The fourth section summarizes the new algorithm.

## II. THEORY AND METHOD

This method is suitable for point cloud splicing when there are few or no feature points on the surface to be welded. The flow chart for the weld identification algorithm is shown in Figure 2. When scanning the workpiece to be welded, the overall point cloud data cannot usually be obtained at once because of the large size of the workpiece or occlusion by other pipes. In this paper, the workpiece (a pipe) has quite a featureless surface, so the surface is labeled with marker points to increase the accuracy of point cloud splicing, as shown in Figure 3. As well as ICP, other common point cloud splicing algorithms include the swarm intelligence

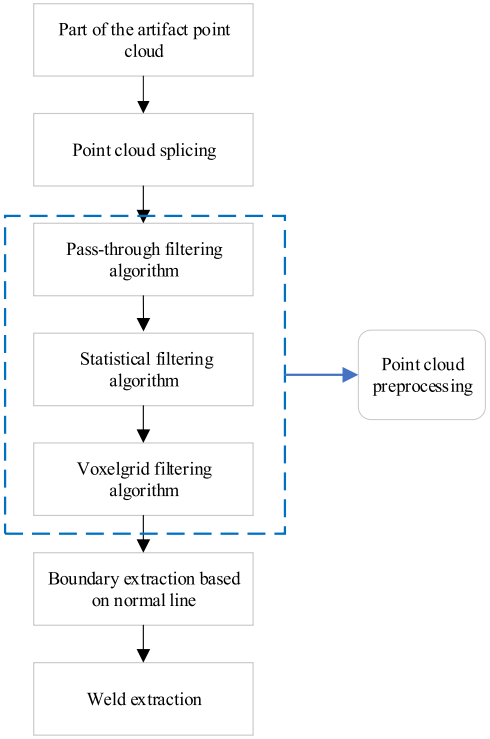


**FIGURE 2.** Flow chart for the spatial closed weld identification algorithm.

**FIGURE 3.** Applying marker points to the surface of the workpiece.

optimization algorithm, and the Normal Distribution Transform algorithm [14]. Compared with the other two algorithms, the ICP algorithm has a more accurate registration effect and does not require segmentation of the point cloud, which greatly improves the computational efficiency.

After the point cloud is spliced, it must be preprocessed. The purpose of point cloud preprocessing is to minimize the effects of noise points, outliers, holes, etc., so that high-level applications such as feature extraction, registration, surface reconstruction, and visualization can be performed better. The originally acquired point cloud contains discrete points, including marked points, and environmental noise, so the point cloud filtering algorithm is used to preprocess the point cloud. First, the point cloud acquired has a limited distribution on the Z axis, so the through filter is used to quickly remove background points, that is, outliers. Second, statistical filtering is used to filter out other outliers from the point cloud. Because the subsequent steps need to estimate the surface normal of the point cloud, different point cloud densities

will complicate the estimation of the surface normal of the point cloud, which will affect the accuracy of the algorithm. Therefore, statistical filtering is selected to smooth the point cloud data. Finally, the VoxelGrid filtering algorithm is used to reduce the number of points in the cloud to improve the subsequent weld extraction efficiency while retaining the point cloud features.

After the point cloud is processed, the extraction of the weld from the point cloud can take place. The welds in this paper comprise point cloud boundary points and are points on a continuous plane. The boundary can be regarded as the point at which the line perpendicular to the point cloud surface is discontinuous. The boundary extraction algorithm based on the normal line is first used to extract the weld seam. This preliminary weld seam is then combined with coordinate constraints to obtain the point cloud for the weld seam.

### A. POINT CLOUD SPLICING

After getting more point cloud data, the data must be unified to the same coordinate system to form a complete point cloud [15]. A rigid body transformation matrix must be calculated to rotate and translate the point clouds and ensure the corresponding parts of the pieces coincide as much as possible [16]. In other words, the transformation matrix is optimized, so that the overlap area between similar pieces of the point cloud data sets is maximized or the distance between the overlapping areas is minimized.

Set the two point clouds to be merged as A and B, define A as the baseline data point set, and take $A_i$ point in A. Find the nearest point $B_i$ in B and form a set of corresponding points $(A_i, B_i)$. There is a definite set of R and T for the two points, but the optimum set of R and T must be found to maximize the matching of point pairs. A total of $n$ pairs constitute $n$ equations $(A_i, B_i)$, and an iterative algorithm is adopted to convert point set B to point set $B'$ by a set of transformation relations. Define $E$ to be calculated as

$$E_d(R, T) = \frac{1}{n}\sum_{i=1}^{n}(R \cdot B_i + T - A_i)^2, \tag{1}$$

where $R$ represents the rotation matrix and $T$ represents the translation matrix.

### B. POINT CLOUD PROCESSING

Before point cloud feature extraction, the obtained point cloud data should be processed, and the point cloud pretreatment process must consider the specific point cloud situation. The first step is to remove the point cloud background, and then the point cloud noise reduction is carried out by the filtering algorithm. The commonly used filtering algorithms include passthrough filtering, voxel filtering, statistical filtering, and radius filtering algorithms [17]. Finally, combined with point cloud data, a subsampling algorithm is adopted to reduce point cloud data, facilitating feature extraction, surface reconstruction, visualization, etc. Furthermore, this method improves the speed of point cloud computing in the later stages [18].

#### 1) BACKGROUND POINT REMOVAL BASED ON PASSTHROUGH FILTERING

Because of the influence of equipment accuracy, operator experience, and environmental factors, the point cloud data contains other object point cloud information and some noise points [19]. Therefore, because the acquired point cloud information inevitably contains environmental information of no interest, the artifact point cloud information must be removed. The collected workpiece point cloud spreads over a wide range of X and Y. However, the Z direction points are distributed within a limited range, so passthrough filtering is adopted to quickly cut off outliers in the Z direction [20].

To do this requires setting the three-dimensional range of point cloud, judging whether the coordinates of the three dimensions of point cloud are within the set range, retaining the points within the set range, and finally getting the cluster of point cloud points after coarse processing [21]. The set of original point clouds is $Q_1$, $Q_1 = \{q_1, q_2, \cdots q_n\}$, in which $n$ represents the number of original data points in the point cloud; the point cloud relative to pixel coordinates is obtained and expressed as $q_i = (x_i, y_i, z_i)$. The whole scanning space takes the pixel coordinate system as its origin. Then the spatial coordinate system

$$\begin{cases} X_{\min} \le x_i \le X_{\max} \\ Y_{\min} \le y_i \le Y_{\max} \\ Z_{\min} \le z_i \le Z_{\max} \end{cases}$$

is established to obtain the range of values of the point cloud space, where $X_{\min}, X_{\max}, Y_{\min}, Y_{\max}, Z_{\min}, Z_{\max}$ represent the maximum and minimum values of the spatial coordinates of the point cloud. According to the coordinates of outliers or target workpiece, the filter range of the passthrough filter is set so that the points that meet the required coordinates can be saved [22], precisely

$$\begin{cases} X_l \le x_i \le X_h \\ Y_l \le y_i \le Y_h \\ Z_l \le z_i \le Z_h, \end{cases}$$

and the point cloud $Q_2$, $Q_2 = \{q_a, q_b, \cdots q_j\}$ is obtained.

#### 2) OUTLIER REMOVAL BASED ON STATISTICAL FILTERING

After the passthrough filtering, there will still be outliers in the point cloud, and errors will be caused when the weld is extracted [23]. Therefore, outliers need to be removed. Statistical filtering involves forming a set of the closest $k$ points around each individual point in the point cloud and then calculating the average distance from the individual point to the others in the set. This average distance is then compared with the overall distribution of the average distances for all other individual points from their corresponding closest $k$ points [24]. This distribution is fitted to a Gaussian, and the mean value and standard deviation of the overall distribution are obtained. The values of mean and variance are referred to in order to set the range of points to be removed [25]. Any points outside the range are regarded

as outliers and removed from the original point cloud [26]. Picture 4 shows the steps of the statistical filtering algorithm.

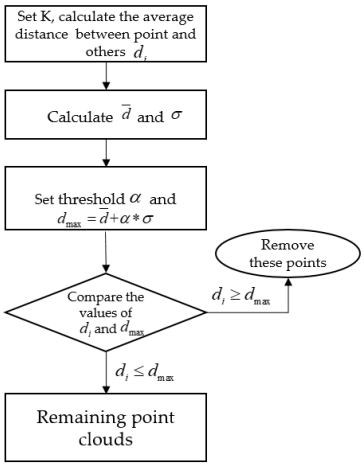


**FIGURE 4.** Steps of the statistical filtering algorithm.

(1) The processed point cloud is set as $Q_2$, and the average distance between each point and the $k$ points in its neighborhood is calculated.

$$d_i = \frac{\sum_{j=1}^{k} \sqrt{(x_i - x_j)^2 + (y_i - y_j)^2 + (z_i - z_j)^2}}{k}, \quad (2)$$

where $(x_i, y_i, z_i)$ is the coordinates of the target point and $(x_i, y_i, z_i)$ are the coordinates of $k$ points in the target point field.

(2) Calculate the mean value $\overline{d}$ and standard deviation $\sigma$ of the overall distribution of average distances, $d_i$.

$$\overline{d} = \frac{\sum_{i=1}^{n} d_i}{n} \quad (3)$$

$$\sigma = \sqrt{\frac{1}{n} \sum_{n=1}^{n} (d_i - \overline{d})^2} \quad (4)$$

(3) Set filtering threshold $d_{\max}$ based upon the mean value and standard deviation.

$$d_{\max} = \overline{d} + \alpha \cdot \sigma, \quad (5)$$

where $\alpha$ is the proportionality coefficient.

(4) Point cloud search, judge the relationship between the corresponding value $d_i$ of a single point in the cloud and the filtering threshold value, delete points whose $d_i$ is larger than the threshold value, output the remaining point cloud, and set it as $Q_3$.

#### 3) POINT CLOUD DOWNSAMPLING BASED ON VOXELGRID FILTERING

Subsampling of point clouds based on the VoxelGrid filter reduces the number of points in the point cloud. The initial point cloud is divided into a voxel grid, which contains N voxels. The center of gravity of each voxel in the grid is obtained, and is used to replace all points in that voxel [27]. The number of points in the original point cloud is reduced by a factor of N. The voxel size in the voxel grid must be appropriate, because otherwise the original point cloud shape features cannot be maintained [28].

The specific steps are as follows.

(1) The maximum and minimum values of X, Y and Z on the coordinate axes of the original point cloud are obtained.

(2) Calculate the point cloud length, width, and height $l_x, l_y, l_z$ according to the maximum and minimum values on the X, Y and Z coordinate axes,

$$\begin{cases} l_x = x_{\max} - x_{\min} \\ l_y = y_{\max} - y_{\min} \\ l_z = z_{\max} - z_{\min}. \end{cases} \quad (6)$$

(3) Set the voxel side length. The three coordinate axes are divided into $M$, $N$ and $L$ parts, and the point cloud is divided into a $M \times N \times L$ grid.

$$sum = M * N * L \begin{cases} M = \left\lfloor \frac{l_x}{cell} \right\rfloor \\ N = \left\lfloor \frac{l_y}{cell} \right\rfloor \\ L = \left\lfloor \frac{l_z}{cell} \right\rfloor, \end{cases} \quad (7)$$

where $\lfloor * \rfloor$ represents rounding down to the nearest integer, and *sum* represents the total number of voxels in the grid.

(4) Number each voxel in the voxel grid $(i, j, k)$; this tracks the voxel to which each point in the point cloud belongs.

$$\begin{aligned} i &= \left\lfloor \frac{(x_i - x_{\min})}{cell} \right\rfloor \\ j &= \left\lfloor \frac{(y_i - y_{\min})}{cell} \right\rfloor \\ k &= \left\lfloor \frac{(y_i - y_{\min})}{cell} \right\rfloor \end{aligned} \quad (8)$$

(5) Calculate the center of gravity of each voxel and replace the voxel in the point cloud with this value. If the barycenter point does not exist, the data point closest to the barycenter in the cell is used to replace all the points in the cell, and finally, the point cloud simplification process is completed. The obtained point cloud is set as $Q_4$.

$$c_{ijk} = \frac{1}{k} \sum_{i=1}^{k} p_i, \quad (9)$$

where $c_{ijk}, p_i, k$ are the center of gravity, data points and the number of voxels in the voxel grid.

### C. WELD EXTRACTION

The feature lines in a point cloud image include ridgelines and valley lines, contour lines, boundary lines, material edge lines, and others. There are two types of methods commonly used to extract these features, one based on normal vectors

and another based on curvature [29]. The welds belong to a contour line feature in the local point cloud, so the PCL:: Boundary Estimation tool from the PCL library was used. The resulting boundary point cloud is segmented using Geomagic Studio software, and the 3D weld seam is finally obtained.

The boundary extraction method, based on the normal vector, is used to judge whether each point in the point cloud is a boundary point or not according to the vector angle of projection between the point in the point cloud and other points in the field in the tangent plane. If the angle between two projection vectors is much larger than the angle between other vectors, the point is designated as a boundary point [30]. The specific steps are as follows:

(1) The normal line at each point in the point cloud can be regarded as the normal line to the approximate tangent plane which includes the unit point cloud. Let the coordinate of the point in the cloud being considered be $P_0\,(x_0, y_0, z_0)$ and the points in its neighborhood be $P_i\,(x_i, y_i, z_i)$, $(i = 1, 2, \cdots n)$. Because it is an approximate fitting plane, the least square method is used for fitting. Let the plane equation to be fitted be

$$\begin{cases} ax + by + cz = d(d \geq 0) \\ a^2 + b^2 + c^2 = 1. \end{cases} \tag{10}$$

The distance from any point to the plane is expressed as

$$d_i = |ax + by + cz - d|\,. \tag{11}$$

Finding the best fitting plane then requires finding the extremum, $e = \sum_{i=1}^{n} d_i^2 \rightarrow \min$.

$$f = \sum_{i=1}^{n} d_i^2 - \lambda\left(a^2 + b^2 + c^2 - 1\right) \tag{12}$$

Take the partial derivatives with respect to a, b and c, we obtain

$$\begin{pmatrix} \sum \Delta x_i \Delta x_i & \sum \Delta x_i \Delta y_i & \sum \Delta x_i \Delta z_i \\ \sum \Delta x_i \Delta y_i & \sum \Delta y_i \Delta y_i & \sum \Delta y_i \Delta z_i \\ \sum \Delta x_i \Delta z_i & \sum \Delta y_i \Delta z_i & \sum \Delta z_i \Delta z_i \end{pmatrix} \begin{pmatrix} a \\ b \\ c \end{pmatrix} = \lambda \begin{pmatrix} a \\ b \\ c \end{pmatrix}. \tag{13}$$

That is, $Ax = \lambda x$. The equation is transformed into the problem of finding the eigenvalues and eigenvectors of matrix $A$. Matrix $A$ is the covariance matrix of N points. $(a, b, c)^T$ is an eigenvector of the matrix, and the plane equation $(a, b, c)^T$ of point $(x_0, y_0, z_0)$ can be obtained.

(2) After obtaining the equation for the approximate fitting plane, we then need to find the vertical lines which intersect the plane, including points $P_i\,(i = 0, 1 \cdots n)$, at the points $P_i'\left(x', y', z'\right)\,(i = 0, 1 \cdots n)$. The normal vectors are then $PP'$ and the plane is $\overline{n} = (a, b, c)$, so the parametric equation of $PP'$ can be expressed as

$$\begin{cases} x = x_i - at \\ y = y_i - bt \\ z = z_i - ct. \end{cases} \tag{14}$$

Point $P_i'\left(x', y', z'\right)\,(i = 0, 1 \cdots n)$ is the intersection point of the line $PP'$ and the fitted plane, and $P'$ is inserted into the plane equation:

$$t = \frac{ax_i + by_i + cz_i - d}{a^2 + b^2 + c^2}. \tag{15}$$

Plug $t$ into the equation (14), the tangent plane equation of the projection point $P_i'\left(x', y', z'\right)\,(i = 0, 1 \cdots n)$ can be obtained.

(3) Normal vector screening of projection points. The projection point of point $P_k' = \left\{p_1', p_2' \cdots p_k'\right\}$ is $P_i'\left(x', y', z'\right)\,(i = 0, 1 \cdots n)$, so $k$ vectors, $P_0'P_1', P_0'P_2', \cdots, P_0'P_k'$ are obtained. The maximum value of the included angle of $k$ vectors is compared with the threshold value. The threshold can be a default parameter. If the value is greater than the set threshold, $P_0$ can be judged as the boundary point. Similarly, the set of boundary points $M$ can be obtained repeatedly.

After obtaining all the boundary information of the workpiece to be welded, the boundary of the weld point cloud is far away from the other point clouds. By choosing an appropriate set of coordinate constraints, the weld point cloud can be separated. Thus, finally, a point cloud containing only the closed weld seam is obtained.

## III. EXPERIMENT

### A. WELD EXTRACTION OF THE CONNECTING PIPE

An experimental platform, as shown in Figure 5 (a), was built to verify the algorithm proposed in this article. The experimental platform is divided into a robotic arm system, a vision system, and a computer processing system. The vision system is installed on the flange at the end of the robotic arm. The point cloud of the workpiece is extracted by the vision system, the parameters of which are shown in Table 1. Figure 5(b) is the experimental flowchart. First, the vision system acquires multiple workpiece point cloud images through the movement of the robotic arm, and then the computer processing system completes the splicing of the workpiece point cloud, processing of the point cloud and extraction of the welding seam, using the algorithms proposed in this paper. The welding seam selected for the experiment is a seam connecting to a pipe, as shown (with added marker points) in Figure 3.

**TABLE 1. Relevant parameters of the 3D scanner.**

| Technical parameters | Numerical |
|---|---|
| Resolution ratio | 1296*966 pixels |
| Measuring range | 640mm |
| Accuracy of measurement | $\pm$ 0.020mm |
| Scanning mode | non-contact |

#### 1) POINT CLOUD SPLICING

Figure 6 shows the acquired point cloud images to be spliced. According to the precision requirements, the conditions at which iteration will terminate are defined. When $E$ is less than $1 \times 10^{-3}$, the iteration will be aborted, and the optimal transformation matrix can be obtained. From the

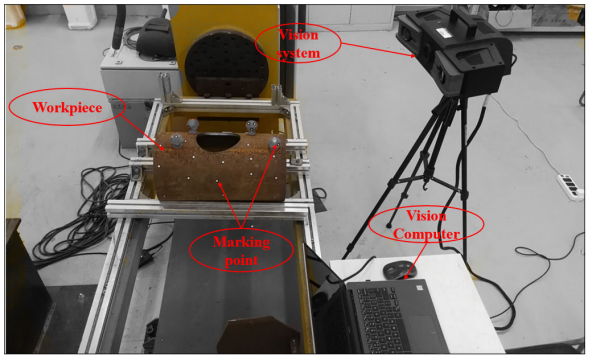


(a)

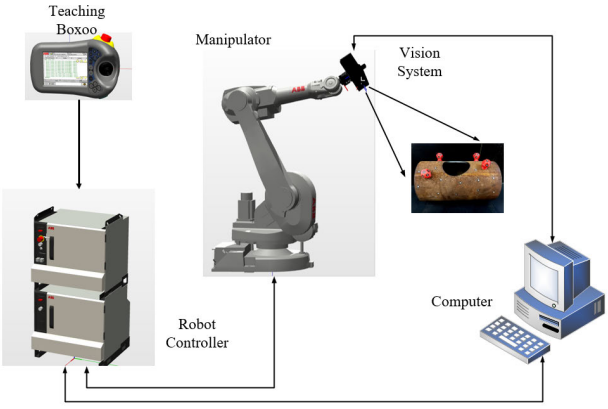


(b)

**FIGURE 5.** The experimental system, (a) experimental platform for weld extraction; (b) experimental flowchart.

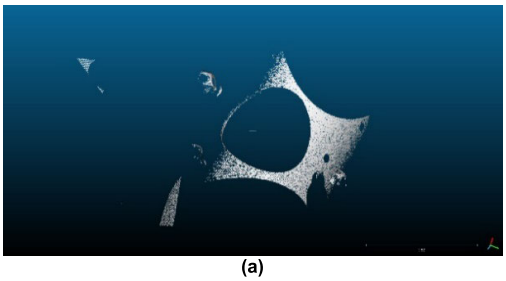

(a)

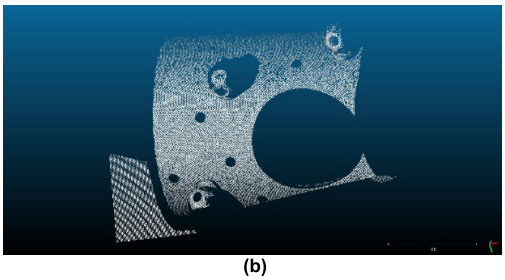

(b)

**FIGURE 6.** Clouds of points to be spliced: (a) Point cloud 1 to be spliced; (b) Point cloud 2 to be spliced.

transformation matrix, point cloud splicing could be realized. Figure 7 shows the workpiece point cloud after point cloud splicing.

$$\begin{bmatrix} R & T \\ 0 & 1 \end{bmatrix} = \begin{pmatrix} 0.649 & -0.748 & -0.137 & -37.764 \\ 0.748 & 0.664 & -0.139 & -56.438 \\ 0.137 & 0.139 & 0.981 & -16.690 \\ 0.000 & 0.000 & 0.000 & 1.000 \end{pmatrix} \quad (16)$$

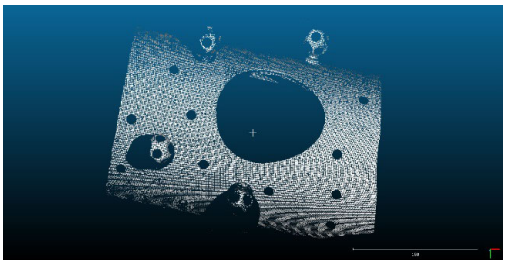

**FIGURE 7.** Point cloud map after splicing.

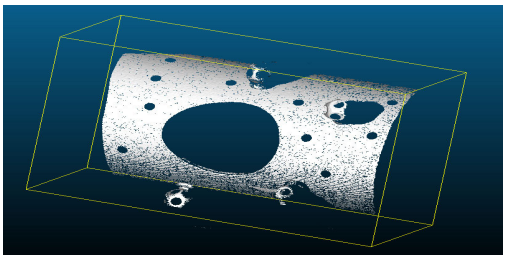

(a)

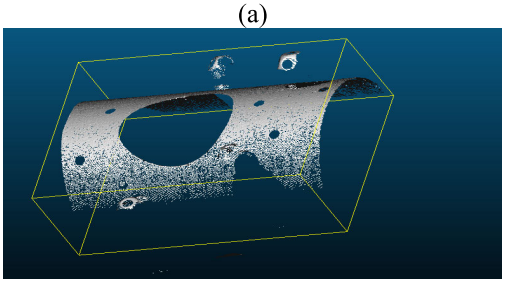

(b)

**FIGURE 8.** Extreme coordinate points. (a) the extreme points on the point cloud; (b) the extreme points on the workpieces.

### 2) POINT CLOUD PROCESSING

Figure 8(a) shows the extreme coordinate points on the point cloud. And Figure 8(b)shows the extreme points on the workpieces. The coordinates of the extreme points in all three directions were:

$$\begin{cases} -184.835 \le x_i \le 258.630 \\ -169.781 \le y_i \le 218.540 \\ -64.555 \le z_i \le 140.973. \end{cases}$$

Table 2 give the extreme coordinates of the point cloud and the workpiece, respectively, on the X, Y and Z axes.

In combination with the point cloud coordinates of the workpiece, the scope of passthrough filtering is:

$$\begin{cases} -143.988 \le x_i \le 182.041 \\ -86.043 \le y_i \le 156.248 \\ -55.365 \le z_i \le 52.130. \end{cases}$$

Figure 9 shows the point cloud image after passthrough filtering, which reduced the number of points from 120,887 to 115,607.

To remove points from the point cloud using statistical filtering, K points for need to be determined for each point

**TABLE 2.** Coordinate range of point cloud extrema.

| The extreme coordinate points | | X | Y | Z |
|---|---|---|---|---|
| The extreme coordinate points on the point cloud | Max | 258.630 | 318.540 | 140.973 |
| | Min | -184.835 | -169.781 | -140.973 |
| the extreme coordinate points on the workpieces. | Max | 182.041 | 156.248 | 52.248 |
| | Min | -143.988 | -86.043 | -55.365 |

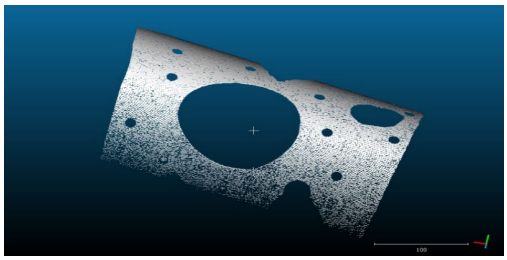

**FIGURE 9.** Point cloud image after passthrough filtering.

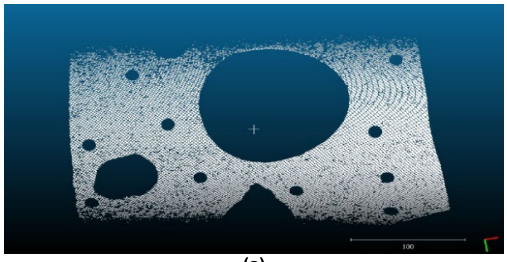

(a)

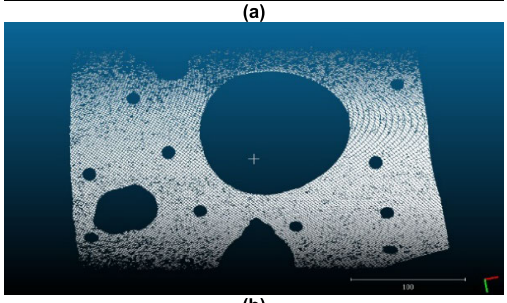

(b)

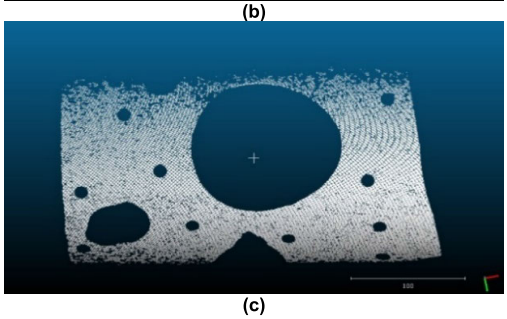

(c)

**FIGURE 10.** Point cloud images after statistical outlier removal using different K values: (a) K = 3; (b) K = 5; (c) K = 10.

in the point cloud, and the average distance between each point in the point cloud and each of its corresponding K points calculated. Figure 10 shows the point cloud after statistical filtering when K = 3, K = 5, and K = 10.

When K = 10, defects appear in the upper part of the weld point cloud, implying that too many points have been

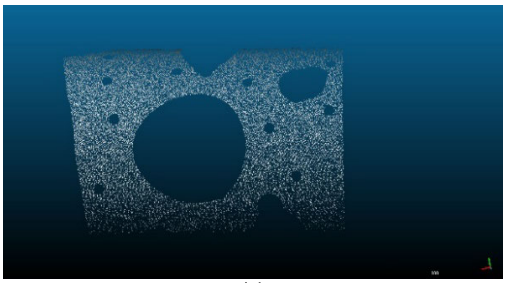

(a)

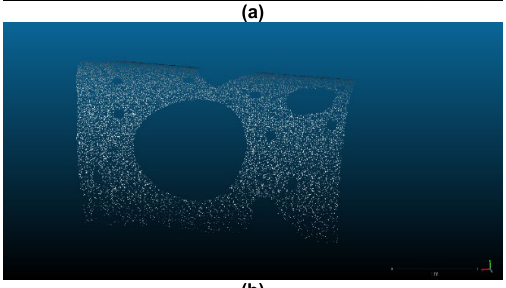

(b)

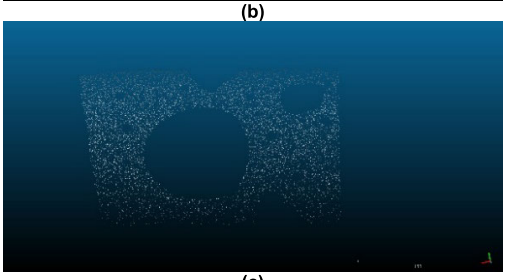

(c)

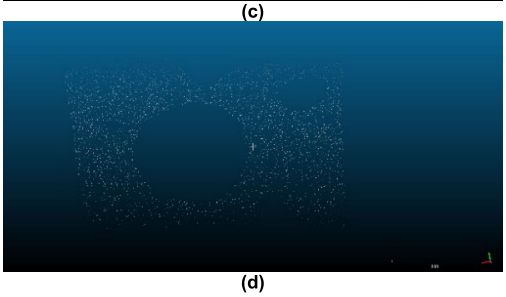

(d)

**FIGURE 11.** Point cloud subsampling results. (a) Cell = 1, point cloud with 54,038 points; (b) Cell = 2, point cloud with 30,131 points; (c) Cell = 3, point cloud with 13,101 points; (d) Cell = 4, point cloud with 6,223 points.

removed. However, when K = 5, the weld point cloud remains intact, so K = 5 was used.

Voxel filtering was used to reduce the number of points – the first step is to set the number of voxels. Figure 11 shows the results of point cloud subsampling. Picture (c) retains characteristic information while reducing the number of point clouds, so cell = 3 is used.

### 3) WELD EXTRACTION

After using the normal-based boundary extraction algorithm, Fig.12 shows the boundary of the workpiece containing the weld.

The edge information of the workpiece containing the weld seam was extracted from the point cloud [31], and then those points on the workpiece side of the boundary were used to obtain the weld point cloud, as shown in Figure 13.

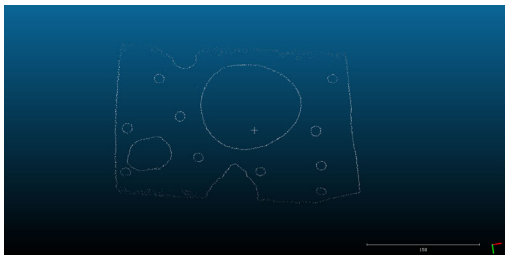

**FIGURE 12.** Edge extraction of weld workpieces.

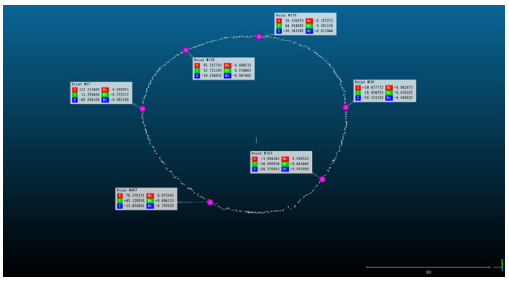

**FIGURE 13.** Cloud map of the weld points.

There were 526 points in the final weld point cloud. Some point cloud coordinates are shown in Table 3, and the remaining point cloud coordinates are shown in Appendix.

**TABLE 3.** Coordinates of weld point cloud.

| Number | X | Y | Z |
|---|---|---|---|
| 1 | 109.725 | -5.395 | 35.059 |
| 2 | 109.851 | -6.005 | 34.821 |
| 3 | 110.235 | -5.366 | -5.172 |
| ... | ... | ... | ... |

To verify the accuracy of the weld point cloud, the least squares method was used to fit the point cloud. The error of the discrete points relative to the fitting curve was calculated and the sum of its squares minimized, and then the final similar surface is fitted. The fitted curve is shown in Figure 14. The value of R-squared is 0.9998, which indicates that the model fits the data well. The method proposed in this paper for the extraction of a spatially complex surface produces a continuous curve on a smooth surface, which is critical for welding to be effective.

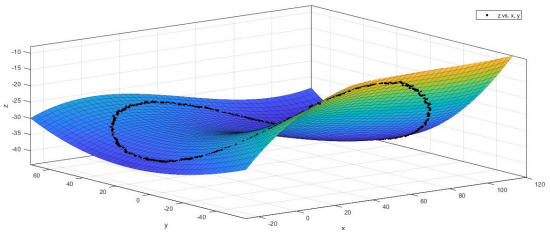

**FIGURE 14.** Fit weld curve.

### B. ERROR ANALYSIS

To improve the welding accuracy for the complicated weld seam at the junction of pipelines or pressure vessels, a method to identify and extract D type welding seam was proposed and tested. The test shows that the method can accurately extract the weld and obtain its spatial coordinates relative to the camera coordinate system. Marker points were applied to the relatively featureless surface to improve the precision when splicing the original point clouds.

The maximum spatial error is estimated as 0.4 mm. The main errors come from camera calibration, point cloud splicing and weld plane fitting. The error of the camera calibration process is 0.5 pixels. Point cloud splicing and curve fitting errors are shown in Table 4. Table 4 shows the errors in X, Y and Z directions for the weld splicing models with and without marked points. The accuracy of point cloud splicing is improved by more than 40% using marker points. The experimental accuracy of the proposed method is sufficient to meet the requirements for actual welding.

**TABLE 4.** Point cloud processing errors.

| Method | | RMSE(mm) X | Y | Z |
|---|---|---|---|---|
| point cloud splicing | without marking point | 0.386 | 0.289 | 0.337 |
| | With marking point | 0.219 | 0.157 | 0.238 |
| weld plane fitting | | 0.149 | 0.115 | 0.179 |
| RMSE: Root Mean Squared Error | | | | |

### C. COMPARISON WITH EXISTING METHOD

Existing methods to identify complex surface welds in space use 3D reconstruction based on binocular vision [32]. Images from binocular cameras are processed to obtain the weld shape, and then the two cameras are matched based on the feature points of the weld, and the three-dimensional coordinates of the weld are finally obtained. We compared the effectiveness of this approach to that of the algorithm proposed in this paper.

Because of the limitations of the field of view of the binocular camera, it is difficult to extract the closed weld. During the comparison test, one field of view of the binocular camera was selected for welding seam extraction. The accuracy and speed of weld extraction are two tests of the effectiveness of the algorithm.

Table 5 and Table 6 show the calculated results for these two methods. The point cloud algorithm adopted in this paper is more efficient than binocular stereo matching. The proposed method more accurate than the existing method, in all three directions; in particular, the accuracy of the proposed method is 28.2% better in the X direction. And the curvature of the workpiece causes the difference in accuracy in all three directions.

**TABLE 5.** Algorithm accuracy.

| Method | RMSE(mm) X | Y | Z |
|---|---|---|---|
| The proposed method | 0.326 | 0.289 | 0.383 |
| The existing method | 0.418 | 0.357 | 0.456 |
| The improvement ratio | 28.220% | 19.048% | 16.009% |
| RMSE: Root Mean Squared Error; | | | |

**TABLE 6. Algorithm speed.**

| Case | Method | Running time(ms) |
|---|---|---|
| 1 | The proposed method | 1135 |
| 2 | The existing method | 2369 |
| The improvement ratio | | 52.089% |

$$The\ improvement\ ratio = \frac{T(The\ existing\ method) - T(The\ proposed\ method)}{T(The\ existing\ method)} \times 100\%$$

T is the running time.

The running time of the proposed method is 52.1% less than that of the existing methods. This is because our new algorithm greatly reduces the number of points in the point cloud through voxel filtering, which also improves the efficiency of subsequent curve fitting. The algorithm proposed in this paper is both more accurate and faster than existing methods.

Because the extraction of a spatially closed point cloud requires a 360-degree field of view, it is more convenient to splice through point clouds than through images. Moreover, the method based on point clouds can not only solve the three-dimensional position problem but also obtain the weld pose information. The algorithm proposed in this paper is also more suitable for complex weld trajectories and has better adaptability.

## IV. CONCLUSION

In this article, we propose a method for extracting D-type welds, such as those used to attach connections to pressure vessels and pipelines.

(1) A point cloud recognition method for D-type welds is proposed. Experiments have demonstrated the effectiveness of the method. Compared with the existing welding seam extraction methods, the algorithm in this paper not only improves the accuracy in three coordinates, 28.2% in X direction,19.0% in Y direction,16.0% in Z direction, but also reduces the running time by 52.1%. The different curvatures of the workpiece surface lead to differences in accuracy in the three directions. If the camera is calibrated on a curved surface, the accuracy of the three directions can be kept constant.

(2) This paper proposes a point cloud splicing method for workpieces lacking features. The accuracy of point cloud splicing improved by 42.3% when the markers were used.

(3) The coordinate information of the weld point cloud obtained in this paper can be directly converted to the base coordinate system of the welding robot through calibration of the manipulator with the vision system. This method provides a real-time method for automatic welding of pressure vessels.

(4) Whether the method in this paper can be applied to fillet welds and T-shaped welds should be further studied. The accuracy and efficiency of the algorithm should also be further improved to ensure real-time welding performance.

## APPENDIX

The final point cloud coordinates have been uploaded to Git, at https://github.com/gobletjie/MDPI-metals.

## ACKNOWLEDGMENT

The authors thank Kate Nairn, Ph.D. from Liwen Bianji, Edanz Editing China (www.liwenbianji.cn/ac), for editing the English text of a draft of this manuscript. They thank Wuhan Vision Technology Company for its support of experimental equipment.

## REFERENCES

[1] Y. C. Chen, "Welding technology of steel pressure vessel," in *Machinery Industry Press*, 2nd ed. Beijing, China: Machinery Industry Press, 2007, pp. 1–30.

[2] Y. Kong and M. Dai, "Three-point weld location technology with robot structured light vision," *Weld. J.*, vol. 18, no. 3, pp. 60–63, Sep. 1997.

[3] C. Li, "Research on welding workpiece identification and welding trajectory correction method based on machine vision," *South China Univ. Technol.*, vol. 36, no. 6, pp. 57–60, Jun. 2015.

[4] Y. D. Wang and X. Q. Lv, "Stereo matching of weld image based on binocular vision," *J. Shanghai Univ. Electr. Power*, vol. 35, no. 2, pp. 175–180, Apr. 2019, doi: 10.3969/j.issn.1006-4729.2019.02.015.

[5] G. Wang, N. Li, and S. Li, "Enhanced histogram feature descriptor for automated point cloud registration," in *Proc. 35th Chin. Control Conf. (CCC)*, Jul. 2016, pp. 7032–7037, Chengdu, China, doi: 10.1109/ChiCC.2016.7554466.

[6] S. Ji, Y. Ren, Z. Ji, X. Liu, and G. Hong, "An improved method for registration of point cloud," *Optik*, vol. 140, pp. 451–458, Jul. 2017, doi: 10.1016/j.ijleo.2017.01.041.

[7] D. F. Liu, H. W. Liao, N. Dai, and X. S. Cheng, "Research and implementation of scattered point cloud denoising algorithm," *J. Southeast Univ.*, vol. 37, no. 6, pp. 1108–1112, Nov. 2007.

[8] J. L. Dai and Z. Y. Chen, "Application of ICP algorithm in point cloud registration," *Chin. J. Image Graph.*, vol. 12, no. 3, pp. 517–521, Mar. 2007.

[9] H. Guo, J. Pan, and D. Lin, "Point cloud registration based on real-coded multi-population genetic algorithm," *J. East China Univ. Sci. Technol. Natural Sci.*, vol. 33, no. 3, pp. 733–736, Oct. 2007, doi: 10.14135/j.cnki.1006-3080.2007.05.030.

[10] L. Yan, J. Tan, and H. Liu, "Registraction of TLS and MLS point cloud combining genetic algorithm with ICP," *Acta Geodaetia Cartographica Sinica*, vol. 47, no. 4, pp. 528–536, Apr. 2018, doi: 10.11947/j.AGCS.2018.20170235.

[11] E. Njastad, "Robotsveising med korreksjon fra 3D-kamera," M.S. thesis, Norwegian Univ. Sci. Technol., Trondheim, Norway, 2015.

[12] S. Bredvold, "Robotic welding of tubes with correction from 3D vision and force control," M.S. thesis, Norwegian Univ. Sci. Technol., Trondheim, Norway, 2016.

[13] R. Stéphane and H. Margit, "From in silico to in spectro kinetics of respiratory complex I," *Biochimica Biophysica Acta*, vol. 1817, no. 10, pp. 1958–1969, 2012.

[14] J. Li, X. Gao, and J. Meng, "An accelerated ICP registration algorithm for 3D point cloud data," in *Proc. 9th Int. Symp. Adv. Opt. Manuf. Test. Technol., Opt. Test, Meas. Technol., Equip.*, Beijing, China, vol. 10839, Jan. 2019, Art. no. 1083904, doi: 10.1117/12.2504772.

[15] B. He, Z. Lin, and Y. F. Li, "An automatic registration algorithm for the scattered point clouds based on the curvature feature," *Opt. Laser Technol.*, vol. 46, pp. 53–60, Mar. 2013, doi: 10.1016/j.optlastec.2012.04.027.

[16] Y. Zhang, G. Geng, X. Wei, S. Zhang, and S. Li, "A statistical approach for extraction of feature lines from point clouds," *Comput. Graph.*, vol. 56, pp. 31–45, May 2016, doi: 10.1016/j.cag.2016.01.004.

[17] Y.-C. Chung, I.-F. Su, C. Lee, and P.-C. Liu, "Multiple K nearest neighbor search," *World Wide Web*, vol. 20, no. 2, pp. 371–398, Mar. 2017, doi: 10.1007/s11280-016-0392-2.

[18] W. Shao, Y. Huang, and Y. Zhang, "A novel weld seam detection method for space weld seam of narrow butt joint in laser welding," *Opt. Laser Technol.*, vol. 99, pp. 39–51, Sep. 2018, doi: 10.1016/j.optlastec.2017.09.037.

[19] Y.-X. Liang, G.-Z. Cao, H. Qiu, S.-D. Huang, and S.-Q. Zhou, "Development of the three-dimensional scanning system based on monocular vision," in *Proc. 6th Int. Conf. Power Electron. Syst. Appl. (PESA)*, Hongkong, Dec. 2015, pp. 1–5, doi: 10.1109/PESA.2015.7398908.

[20] G. Zhang, "Novel calibration method for a multi-sensor visual measurement system based on structured light," *Opt. Eng.*, vol. 49, no. 4, Apr. 2010, Art. no. 043602, doi: 10.1117/1.3407429.

[21] M. A. Fischler and R. C. Bolles, "Random sample consensus: A paradigm for model fitting with applications to image analysis and automated cartography," *Reading Comput. Vis.*, vol. 6, no. 6, pp. 726–740, 1987, doi: 10.1016/B978-0-08-051581-6.50070-2.
[22] T. Zhou, "Point clouds registration algorithm based on improved ISS feature points and artificial bee colony algorithm," *J. Tianjin Univ.*, vol. 49, no. 12, pp. 1296–1302, Dec. 2016, doi: 10.11784/tdxbz201509022.
[23] P. Lian and P. Hui, "Improved denoising of point-sampled model based on bilateral filtering," *Comput. Technol. Develop.*, vol. 29, no. 11, pp. 42–46, Nov. 2019, doi: 10.3969/j.issn.1673-629X.2019.11.009.
[24] Y. H. Wang and H. H. Wang, "Rotational-guided optimal cutting-plane extraction from point cloud," *Multimedia Tools Appl.*, vol. 79, pp. 1–23, Dec. 2019, doi: 10.1007/s11042-019-08339-w.
[25] L. Liu, "Research on Kinect dimension measurement method," M.S. thesis, Harbin Inst. Technol., Harbin, China, 2017.
[26] X. Chen and Y. Yang, "Point cloud data segmentation supported by Euclidean clustering algorithm," in *Proc. Bull. Surv. Mapping*, vol. 11, Jul. 2019, pp. 27–31, doi: 10.13474/jcnki.11-2246.2017.0342.
[27] J. Lu, W. Wang, H. Shao, and L. Su, "Point cloud registration algorithm fusing of super 4PCS and ICP based on the key points," in *Proc. Chin. Control Conf. (CCC)*, Guangzhou, China, Jul. 2019, pp. 27–30.
[28] J. Lu, Z. Wang, B. Hua, and K. Chen, "Automatic point cloud registration algorithm based on the feature histogram of local surface," *PLoS ONE*, vol. 15, no. 9, Sep. 2020, Art. no. e0238802, doi: 10.1371/journal.pone.0238802.
[29] T. Lei, Y. Rong, H. Wang, Y. Huang, and M. Li, "A review of vision-aided robotic welding," *Comput. Ind.*, vol. 123, Dec. 2020, Art. no. 103326, doi: 10.1016/j.compind.2020.103326.
[30] Y. Yang, H. Fang, Y. Fang, and S. Shi, "Three-dimensional point cloud data subtle feature extraction algorithm for laser scanning measurement of large-scale irregular surface in reverse engineering," *Measurement*, vol. 151, Feb. 2020, Art. no. 107220, doi: 10.1016/j.measurement.2019.107220.
[31] D. Z. Sun, Z. X. Fan, and Y. R. Li, "Automatic extraction of boundary characteristic from scatter data," *Nature Sci.*, vol. 36, no. 8, pp. 82–84, Sep. 2008, doi: 10.13245/j.hust.2008.08.024.
[32] C. Jiang, "Research on 3D information of weld seam image based on machine vision," M.S. thesis, Southwest Petroleum Univ., Chengdu, Sichuan, China, 2018.

**JIE GAO** received the bachelor's degree from the Wuhan University of Technology, in 2016. He further studied at the Wuhan Institute of Technology, in 2018. His current research interests include machine vision and intelligent manufacturing.

**FANG LI** received the Ph.D. degree from the Huazhong University of Science and Technology, Wuhan, China, in 2008.

From 2009 to 2011, she was a Postdoctoral Research Fellow with the National Institute for Materials Science, Japan. She is currently a Professor and a Doctoral Supervisor of the Wuhan Institute of Technology. Her main research interests include nonlinear optics, ultrafast nanophotonics, and laser processing.

**CONG ZHANG** received the master's degree from the Wuhan Institute of Technology, in 2019, where he is currently pursuing the Ph.D. degree. His research interests include robot control and multi robot coordination.

**WENHAO HE** received the bachelor's degree from the Hubei University of Science and Technology, in 2019. He further studied at the Wuhan Institute of Technology, in 2020. His research interest includes application of lasers.

**JINHU HE** received the bachelor's degree from the Wuhan City College. He further studied at the Wuhan Institute of Technology, in 2020. His research interests include machine learning, and design and manufacturing.

**XUBING CHEN** (Senior Member, IEEE) received the Ph.D. degree in material science and engineering from the Huazhong University of Science and Technology, Wuhan, China, in 2000.

From August 2007 to October 2008, he was a Visiting Scholar with the Worcester University of Technology. He is currently a Professor with the School of Mechanical and Electrical Engineering, Wuhan Institute of Technology, Wuhan. He has published more than 50 peer-reviewed articles. His research interests include robotics and intelligent manufacturing. He is also a member of the Chinese Mechanical Engineering Society and the Robotics Branch of the Chinese Mechanical Engineering Society.